ICARUS **127,** 379–393 (1997)
ARTICLE NO. IS975698

A Baseline Spectroscopic Study of the Infrared Auroras of Jupiter

Hoanh An Lam, Nicholas Achilleos, Steven Miller, and Jonathan Tennyson

Department of Physics and Astronomy, University College London, Gower Street, London WC1E 6BT, United Kingdom
E-mail: s.miller@ucl.ac.uk

Laurence M. Trafton

Department of Astronomy and McDonald Observatory, University of Texas, Austin, Texas 78712

Thomas R. Geballe

Joint Astronomy Center, 665 Komohana Street, Hilo, Hawaii 96720

and

Gilda E. Ballester

Department of Atmospheric, Oceanic and Space Sciences, University of Michigan, 2455 Hayward, Ann Arbor, Michigan 48109

Received August 8, 1996; revised December 2, 1996

We present the results of a spectroscopic study of the H_3^+ infrared emissions of Jupiter, obtained using the United Kingdom Infrared Telescope (UKIRT) on Mauna Kea, Hawaii, during May 3–5, 1993. Although we have obtained data from the whole of the planet, in this paper we concentrate on the auroral regions. Derived H_3^+ temperatures for these vary between 700 and 1000 K, and column densities are of the order of 10^{12} cm^{-2}. There is a strong (anti-)correlation between these parameters, however, that requires the introduction of new variables to characterize the jovian auroras fully. The total H_3^+ auroral emission is presented as a function of central meridian longitude. A simple geometric model of this emission does not describe the data adequately. The integrated infrared auroral emission in each hemisphere is of the order of a few × 10^{12} W, making it comparable to auroral output in the ultraviolet.

INTRODUCTION

When H_3^+ was first observed in the auroral regions of Jupiter in 1988 (Trafton *et al.* 1989) and its spectrum accurately assigned (Drossart *et al.* 1989), planetary astronomers hoped that this fundamental ion would be a sensitive probe of conditions in the jovian atmosphere. So it is not surprising that the first 5 years of H_3^+ astronomy has seen a flurry of activity (see review by Miller *et al.* 1994). The molecule had been predicted to be an important component of the jovian ionosphere (Atreya and Donahue 1976, Atreya 1986, McConnell and Majeed 1991), and its presence had been inferred from Voyager particle data (Hamilton *et al.* 1980). From the standpoint of molecular physics, the detection of the H_3^+ infrared spectrum for the first time outside of the laboratory gave an impetus to both theoretical (Miller and Tennyson 1988, 1989) and spectroscopic (Majewski *et al.* 1989; Lee *et al.* 1991) studies of this ion. It also encouraged (mostly successful) searches for the spectrum in other planets (Trafton *et al.* 1993, Geballe *et al.* 1993).

Drossart and co-workers' (1989) detection was made at 2 μm during a search for the infrared quadrupole transition of molecular hydrogen. At this wavelength, it is the $2\nu_2 \rightarrow 0$ overtone spectrum of H_3^+ that appears, corresponding to a two-quantum vibrational jump. Normally, such overtone spectra, being dipole forbidden in the harmonic oscillator approximation, are an order of magnitude weaker than the corresponding one-quantum fundamental spectrum; however, H_3^+ is pathologically "floppy," in the sense of Sutcliffe and Tennyson (1986), and many normally "forbidden" transitions turn out in theory (Miller *et al.* 1990a) and practice (Xu *et al.* 1992) not only to be allowed, but quite strongly so. Einstein A coefficients for the H_3^+ overtone transitions are typically of the order of 10^2 sec^{-1}, comparable to those for the fundamental (Kao *et al.* 1989). Thus, despite the low abundance of H_3^+ compared with H_2, and the formally "forbidden" nature of the $2\nu_2 \rightarrow 0$ transition, in Jupiter many of the 2-μm H_3^+ lines are in fact stronger than the $v = 1 \rightarrow 0$,S(1) line of molecular hydrogen.

0019-1035/97 $25.00

Nonetheless, at the temperature deduced by Drossart *et al.* (~1100 K), local thermal equilibrium (LTE) predicts that the $v = 1$ level of H_3^+ should have a population ~20 times greater than the $v = 2$ level. Given the similarity of the Einstein A coefficients, this leads to the conclusion that the $\nu_2 \rightarrow 0$ fundamental emission spectrum should be up to an order of magnitude brighter than the overtone. For this reason, after the initial detection, most workers transferred their attention to the region 3 to 4 μm, where the fundamental lines are most accessible.

Maillard *et al.* (1990) and Oka and Geballe (1990) were both able to detect strong fundamental emission at high spectral resolution ($\lambda/\Delta\lambda > 10^4$). Miller *et al.* (1990b), working at moderate resolution ($\lambda/\Delta\lambda \sim 10^3$), were able to measure both the fundamental and overtone spectra in the same night. They concluded that, indeed, the relative intensities of the two bands showed that the $v = 1$ and $v = 2$ levels were populated as might be expected from LTE. This should not, however, be taken to mean that all H_3^+ levels are thermally populated in the conditions that prevail in the jovian ionosphere. For example, Kim *et al.* (1991) have modeled the distribution of H_3^+ levels and conclude that the high Einstein A coefficients make radiative depopulation of vibrationally excited levels competitive with population by collisional excitation. This leads to a relative overabundance of molecules in the ground state, an important conclusion to which we refer later.

The results of the various spectroscopic studies have shown that typical derived auroral ionospheric temperatures can vary between 1100 K (Maillard *et al.* 1990) and 650 K (Oka and Geballe 1990), the latter temperature being rather lower than ''normally'' found. Column densities deduced from both the overtone (Drossart *et al.* 1989) and fundamental (e.g., Ballester *et al.* 1994) emissions, assuming LTE, are of the order of 10^{12} cm^{-2}. It should, however, be emphasized that all the published spectroscopic studies have been carried out at relatively low spatial resolution, typically with beams or pixels covering a few seconds of arc. This converts to ~10^4 km at Jupiter. But the most recent infrared and ultraviolet images of Jupiter's auroras show them to have very narrow bright emission arcs, with less intense, diffuse emission regions superimposed (Satoh *et al.* 1996, Prangé *et al.* 1995, Clarke *et al.* 1995). Locally, therefore, H_3^+ concentrations may be much higher than indicated by the spectroscopic studies, which measure a spatial average over a relatively large area. Added to the ground-state overpopulation, referred to above, it follows that spectroscopically derived column densities should be seen as lower limits.

The work presented here results from a 3-day study of jovian H_3^+ emission carried out using the facility spectrometer CGS4 of the United Kingdom Infrared Telescope (UKIRT), on Mauna Kea, Hawaii. This spectrometer has a long slit with variable pixel size, and typically provides anywhere between 12 and 30 spectra from different locations across the planet, depending on setup and apparent diameter of Jupiter at the time of study. This means that CGS4 spectroscopic studies, while not having the spatial resolution of the infrared cameras now in use, may complement imaging by providing more information about the physical conditions in the jovian ionosphere. They can also be extremely important in producing data on the ionosphere at lower latitudes where imaging is rather insensitive to the low level of IR emission produced. In this paper, however, while we will show some data pertaining to the subauroral latitudes, we concentrate on the region of the planet from the main auroral arc poleward to the limb of the planet.

DATA ACQUISITION AND REDUCTION

Observing Parameters

Spectra of Jupiter were obtained in the region 3 to 4 μm using the UKIRT CGS4 spectrometer with the short-focus (150-mm) camera and the 150-lines/mm grating during the nights of May 3 to 5, 1993 (UT). This setup gave a spectral resolving power of $\lambda/\Delta\lambda \sim 1200$ and a pixel size of $3.08'' \times 3.08''$. At the time of observation, Jupiter's equatorial and polar diameters subtended $44''$ and $42''$, respectively. The sub-Earth latitude of the planet was $-3°$ and the polar position angle 18°. During the 3 nights, the blurring of individual spectral images due to seeing and the telescope's limitations in pointing and tracking was typically $1.5''$, with many images being better than this. For the work reported here, the CGS4 slit was aligned along the central meridian longitude (CML) and the observing technique explained in Ballester *et al.* (1992) was used. Elapse times between spectra were ~10 min, during which Jupiter rotated by 6°.

Wavelength Settings

For much of the range 3–4 μm, H_3^+ studies of Jupiter are made easier by the fact that methane in the planet's stratosphere absorbs much of the incident solar infrared flux. H_3^+ emission, occurring above the homopause, stands out in stark contrast to an otherwise dark planet. Two central wavelength settings were chosen for the work reported here, 3.47 and 4.00 μm. At the shorter wavelength, the setup described above gave a spectral window of 0.19 μm, and at the longer, 0.20 μm. Typical spectral images are shown in Fig. 1. The data obtained are listed in Table I.

The methane band responsible for absorbing sunlight is ν_3, centered on 3.28 μm, with its P branch extending to longer wavelengths. Near 3.47 μm the absorption by methane is almost total right across the planet and H_3^+ emission may be detected at all latitudes (Fig. 1a). The lines are brightest at the polar auroral regions, reducing in intensity

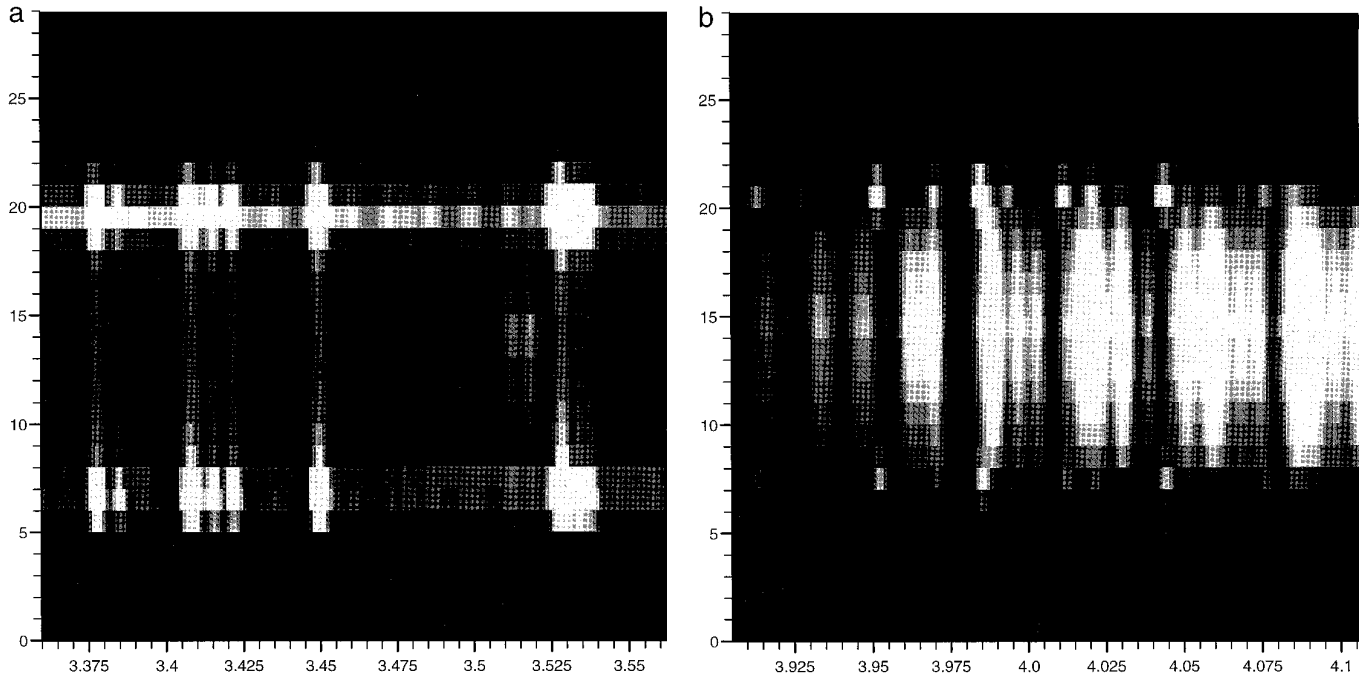

FIG. 1. Spectral images of Jupiter obtained by CGS4 at (a) 3.47 μm and (b) 4.00 μm. The y axis indicates detector position, with the slit aligned along the central longitude meridian with jovian north at the top.

toward the equator. There are other features, not due to H_3^+, that brighten toward the equator, particularly at 3.52 μm (Ballester *et al.* 1994), which have recently been ascribed to reflected solar IR, not totally absorbed by methane (Drossart *et al.* 1996). Thus the 3.47-μm-wavelength region is extremely useful for studying the auroral emission of Jupiter in conjunction with that at lower latitudes (see Ballester *et al.* 1994). But the drawback of this wavelength range is that the H_3^+ lines are a rather random selection, making determination of physical parameters difficult.

Near 4.00 μm, however, a number of H_3^+ Q-branch fundamental lines are available, with J varying from 1 to 6 (Kao *et al.* 1989) (Fig. 1b). The most prominent of these in Jupiter is $Q(3)$ at 3.986 μm. These lines are useful for deriving temperatures (see next section) since they form part of a series whose relative intensities are sensitive to variations in this parameter. This spectral region suffers from the fact that it is relatively far removed from the center of the CH_4 ν_3 band, however, and the absorption of the solar IR is far from complete. This makes it almost impossible to measure the H_3^+ emission at latitudes lower than ~50°, without much higher spectral resolution, since, as the available methane absorption pathlength decreases, reflected sunlight comes increasingly to dominate the spectrum. This spectral region, therefore, is useful only for studying auroral emission.

For both spectral windows, the wavelength scale was fixed with reference to the H_3^+ lines, whose frequencies are now known to better than 0.024 cm^{-1} (Neale *et al.* 1996). This made it unnecessary to allow for the relative motion of Jupiter with respect to the Earth. To divide out the effect of Earth's atmosphere, the jovian spectra were divided by those of the standard star. At the shortest wavelengths, terrestrial methane lines are present. So as to avoid intro-

TABLE I
UKIRT Auroral Data Obtained during 1993

Date	Time (UT)	λ(μm)	CML (System III)
May 3	05:36	3.47	102
	07:11	4.00	160
	07:42	3.47	180
	08:13	4.00	196
	08:32	3.47	210
	09:46	3.47	254
	10:27	4.00	278
	11:37	3.47	324
May 4	05:14	3.47	241
	06:55	4.00	299
	07:33	3.47	325
	08:01	4.00	339
	08:55	3.47	40
May 5	05:09	4.00	26
	05:42	3.47	47
	07:01	4.04	92
	09:11	3.45	174
	09:57	4.00	202

ducing spurious effects into the spectrum where these lines, which are unresolved in our spectra, did not overlap with jovian H_3^+ emission lines, they were first removed from the star spectrum. Only one H_3^+ line, at 2930.169 cm^{-1} (3.413 μm), was partially affected by terrestrial methane, and this was allowed for during fitting (see next section).

DATA ANALYSIS

H_3^+ Temperature and Column Density

To fit H_3^+ temperatures [$T(H_3^+)$] and column densities [$N(H_3^+)$], the flux-calibrated, standard-divided spectra obtained as described above had to be processed further to remove the background emission. In the case of the auroral spectra centered on 3.47 μm, a typical example of which is shown in Fig. 2, the background continuum emission is weak in comparison with the H_3^+ emission, even at the equator (middle spectrum). At the auroral regions, it is hardly noticeable. For these spectra, therefore, the background between the H_3^+ lines was fitted by a fourth-order polynomial. With background thus fixed, $T(H_3^+)$ and $N(H_3^+)$ were fitted using a standard least-squares procedure and a list of line frequencies and Einstein A coefficients from Kao *et al.* (1989), with additions produced by Neale *et al.* (1996). The ortho/para ratio, taken as a variable by Drossart *et al.* (1989), was fixed at 1 : 1, since theoretical considerations show this to be correct (Tennyson *et al.* 1993) and no study of Jupiter has obtained a value significantly different from this.

Figure 3, on the other hand, shows that even at higher latitudes there is a significant background in the 4-μm window, which becomes more pronounced at higher wavelengths. For this region the procedure used by Joseph *et al.* (1992), which uses a scaled equatorial spectrum to simulate the background at higher latitudes, was applied. Given the existence of H_3^+ emission at the equator, this procedure slightly overcompensates for the continuum under the H_3^+ lines. For the 4.00-μm spectra, the background scaling factor, as well as $T(H_3^+)$ and $N(H_3^+)$, was allowed to vary during fitting. Figure 2 shows that the equatorial H_3^+ emission was between 2 and 3% of that of the auroral region at 3.47 μm. Given that the scaling factor for the 4.00-μm equatorial spectra was typically less than 0.1, it is clear that the overcompensation of the continuum background under the H_3^+ lines in this window was negligible, less than 0.5%. To have failed to have corrected for the background, however, would typically have resulted in fitted temperatures ~50 K greater than those reported here.

Figures 2 and 3 show that the fits to the data in the auroral regions were extremely good. Pairs of $T(H_3^+)$ and $N(H_3^+)$ values could be obtained for all the spectra taken. (It should be noted that these parameters are averages over 3.08″ × 3.08″ pixels, which covered an area on the plane at Jupiter approximately 9800 × 9800 km^2 at the time of our observations.) Typical values for these are given in Tables II to V, the units of $N(H_3^+)$ being 10^{12} cm^{-2}. Errors for these two parameters were obtained by fixing one at its fitted value and varying the other until a 2σ standard deviation was produced. The limitations of this process are discussed below. Parameters are given as a function of pixel row number, with the center of the planet generally located in row 13 or 14. As a measure of the relative intensities of the spectra as a function of the position on the slit, we report I(3.533 μm), the intensity of the strongest emission line in the window.

As well as fitting temperatures and column densities (and backgrounds where necessary), the program suite developed by Lam (1995), and used throughout this work, fits the center of each slit pixel, allocating it either a latitude or a height above the limb of the planet (taken at the 0.6-bar level). This is done by adjusting the fitted position of the planet on the slit so as to maximize the emission which appears to come from the disk of the planet, as opposed to that coming from locations apparently above the limb. The computed location is given in the column Lat. (km). From this, the suite also calculates an approximate line-of-sight correction (column headed L.S. in Tables II–V). This was done by assuming a spherical emitting shell of uniform thickness and determining the average pathlength along the line of sight, between this shell's outer and inner boundaries, as a multiplier of the shell thickness. Thus equatorial pixels have a line-of-sight correction of 1.0, rising to 5.0 in the auroral regions. For apparently ''off-planet'' emissions, a line-of-sight correction of 5 was applied, being an average between (1) the large effect produced by the line-of-sight correction for part of the pixel and (ii) pixel filling factor being less than unity. As a result, we also report values of $N(H_3^+)$*, the column density divided by the line-of-sight correction. The related parameters $E(H_3^+)$ and $E(H_3^+)$* are discussed below.

Tables II and III show clearly the relative H_3^+ intensities of the rows spanning the planet. The brightest rows, as expected, are toward the poles, with emission up to 50 times as intense as at the equator. It is clear that the location of the brightest row, as determined by the column Lat. (km), depends critically on the exact positioning of the detector array on the planet. Table II, for example, shows that the brightest northern row was located 183 km above the limb of the planet at CML = 324° on May 3, but Table III gives it at North 66° CML = 325° on May 4. The discrepancy is, however, understandable given that one pixel corresponds to ~9800 km. Similarly, Table III puts the brightest row in the south at 5479 km above the limb, with another bright row at South 66°. This is explicable by bright emission close to the limb of the planet falling on the boundary between two pixels, and thus registering in both. A good indication of the pixel-to-pixel spreading as a result of seeing can be seen by comparing rows 6

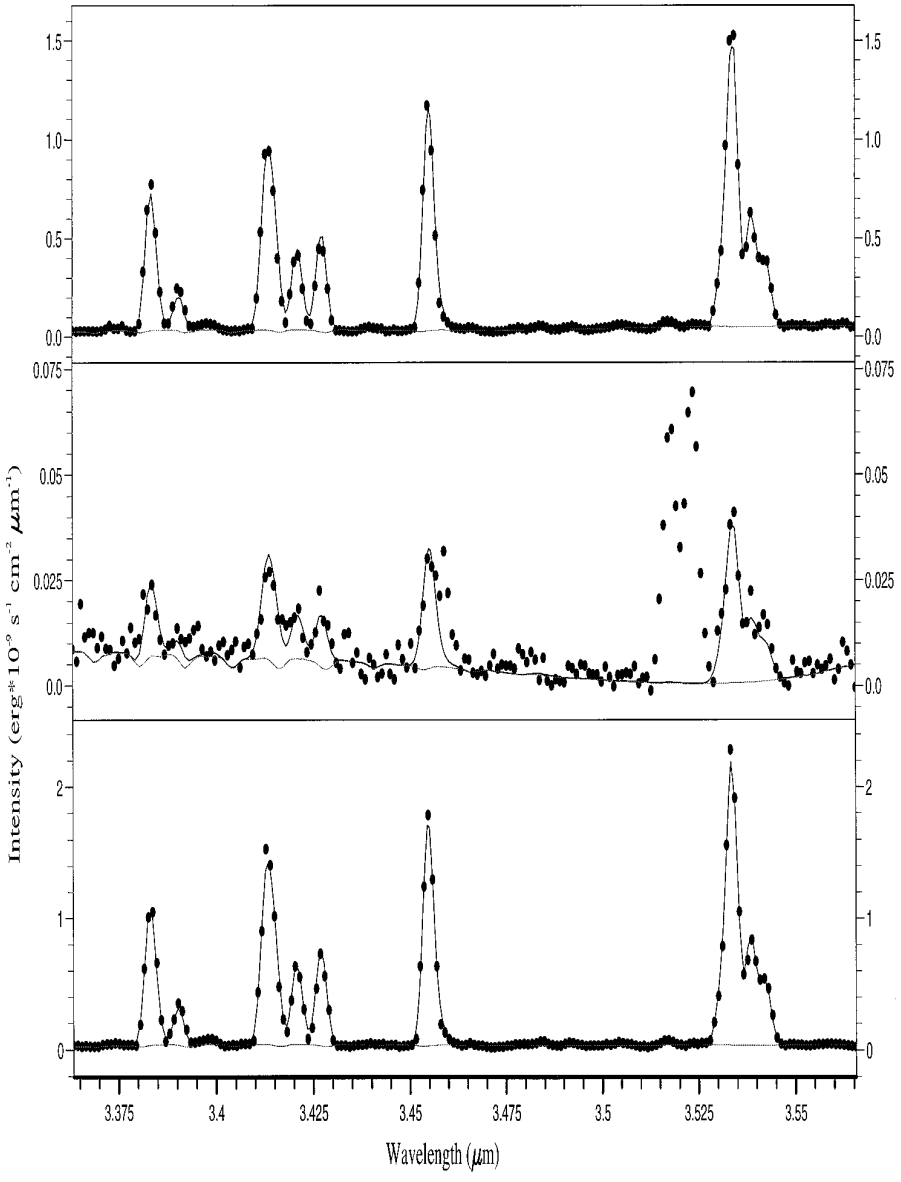

FIG. 2. Typical H_3^+ spectral fits to the data at 3.47 μm, with (a) the northern auroral zone, (b) the jovian equator, and (c) the southern auroral zone. Filled circles, observed spectrum; heavy line, total fitted spectrum; light line, continuum background.

(15,800 km above the limb) and 7 in Table III. This shows that such "leakage" from a bright pixel to its neighbor is not more than 2%.

Tables II and III give temperatures for the northern brightest row (row 20) of 878 and 818 K for May 3 and 4, respectively. But in the south, the temperature on May 3 of 766 K in row 7 had changed on May 4 to 961 K in row 8 and 707 K in row 7. This gives average temperatures, weighted by the relative intensities of the rows, of 839 K for the north and 805 K for the south for the region around CML = 325°. Combining temperatures from Tables IV and V gives average temperatures around CML = 200° of 943 K for the north and 981 K in the south. The tables also show that column densities, after line-of-sight correction, varied from a few $\times 10^{11}$ cm^{-2} to $\sim 1.5 \times 10^{12}$ cm^{-2}. This gives an indication of the possible range of column densities and temperatures that prevailed in the jovian auroral regions during the period of our observations.

It is significant that the fits carried out for the 3.47-μm data generally gave lower temperatures and column densities than those for the 4.00-μm data. For reasons explained above, the 3.47-μm data are considered to be

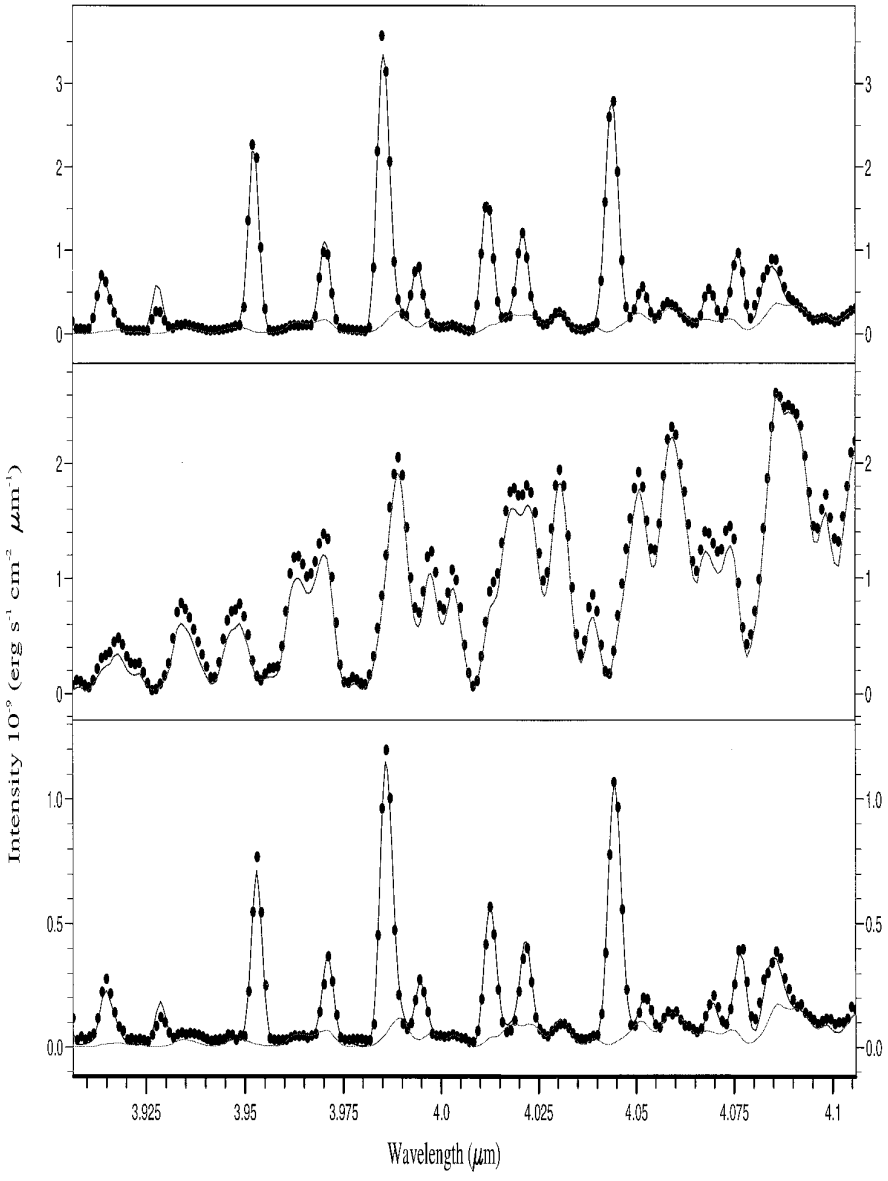

FIG. 3. As in Fig. 2, at 4.00 μm.

less reliable for fixing temperatures. During the period of our study, we therefore conclude that the auroral temperature was toward the higher end of our indicated range. This, in turn, suggests that the pixel averaged column densities in the auroral regions are of the order of a few $\times 10^{11}$ cm^{-2}, and certainly not much in excess of 10^{12} cm^{-2}. Such values are consistent with the predictions of models such as those quoted by Atreya (1986) and of Kim *et al.* (1991), McConnell and Majeed (1991), and Trafton *et al.* (1994), as well as work in progress at University College London.

Figures 4 and 5 show maps of temperature and line-of-sight-corrected column density as a function of jovian location, as determined from all the spectra we obtained. Superimposed on the maps are the loci of the magnetic footprint of the orbit of Io (which maps to field lines that cross the magnetic equator at $6R_J$) and of the last closed field line, as determined from the O6 plus current sheet model of Connerney (1993). Insofar as can be determined from the relatively poor spatial resolution provided by the spectrometer, the auroral regions appear to correspond to zones of higher temperatures than the rest of the planet. Column densities are also much higher. But there are also indications the maps should not be taken too far in isolation from one another. In particular, it is noticeable that in the

TABLE II
3 May 1993: 3.45-μm Dataset Taken at CML of 324

Row	I(3.533 μm) (10^{-13} erg cm^{-2})	Lat. (km)	T(K)	$N(H_3^+)$ (10^{12} cm^{-2})	$E(H_3^+)$ (10^{-3} erg sec^{-1} cm^{-2} sr^{-1})	L.S.	$N(H_3^+)$* (10^{12} cm^{-2})	$E(H_3^+)$* (10^{-3} erg sec^{-1} cm^{-2} sr^{-1})
22	0.32	20,785[a]	996	0.01	4	5.0	0.003	1
21	1.23	10,484[a]	924 ± 120	0.07 ± 0.04	14	5.0	0.01	3
20	22.25	183[a]	878 ± 31	1.32 ± 0.21	218	5.0	0.26	44
19	8.23	56N	639 ± 22	1.92 ± 0.44	65	1.8	1.08	37
18	3.62	42N	699 ± 35	0.57 ± 0.16	31	1.3	0.43	23
17	2.10	30N	808 ± 64	0.18 ± 0.08	21	1.2	0.16	18
16	1.87	21N	774 ± 58	0.19 ± 0.08	17	1.1	0.18	16
15	1.72	12N	756 ± 62	0.21 ± 0.09	18	1.0	0.20	17
14	1.52	4N	812 ± 90	0.14 ± 0.07	16	1.0	0.14	16
13	1.46	4S	744 ± 74	0.18 ± 0.10	13	1.0	0.18	13
12	1.52	12S	755 ± 83	0.16 ± 0.10	13	1.0	0.16	13
11	1.75	21S	833 ± 92	0.14 ± 0.07	18	1.1	0.13	16
10	2.04	30S	766 ± 54	0.21 ± 0.08	19	1.2	0.19	16
9	3.68	42S	757 ± 38	0.39 ± 0.11	33	1.3	0.29	24
8	11.08	56S	891 ± 36	0.64 ± 0.11	111	1.8	0.36	63
7	74.14	183[a]	766 ± 23	7.60 ± 1.29	727	5.0	1.52	145
6	2.10	10,484[a]	584 ± 41	0.94 ± 0.45	18	5.0	0.19	4

[a] Apparent height of pixel center above jovian limb.

TABLE III
4 May 1993: 3.45-μm Dataset Taken at CML of 325

Row	I(3.533 μm) (10^{-13} erg cm^{-2})	Lat. (km)	T(K)	$N(H_3^+)$ (10^{12} cm^{-2})	$E(H_3^+)$ (10^{-3} erg sec^{-1} cm^{-2} sr^{-1})	L.S.	$N(H_3^+)$* (10^{12} cm^{-2})	$E(H_3^+)$* (10^{-3} erg sec^{-1} cm^{-2} sr^{-1})
22	0.67	15,800[a]	784 ± 126	0.06 ± 0.05	6	5.0	0.01	1
21	6.59	5,479[a]	918 ± 41	0.38 ± 0.07	77	5.0	0.07	16
20	42.23	66N	818 ± 39	3.41 ± 0.55	409	2.4	1.42	170
19	4.96	48N	752 ± 60	0.56 ± 0.12	45	1.5	1.38	30
18	2.95	36N	720 ± 68	0.42 ± 0.10	27	1.2	0.34	35
17	1.87	26N	733 ± 30	0.27 ± 0.09	19	1.1	0.24	24
16	1.69	16N	783 ± 29	0.18 ± 0.07	18	1.1	0.16	16
15	1.52	8N	790 ± 64	0.16 ± 0.07	16	1.0	0.16	16
14	1.28	0N	875 ± 46	0.09 ± 0.05	15	1.0	0.09	15
13	1.34	8S	731 ± 144	0.20 ± 0.09	14	1.0	0.20	14
12	1.60	16S	834 ± 12	0.12 ± 0.05	16	1.1	0.12	15
11	1.84	26S	695 ± 45	0.33 ± 0.12	17	1.1	0.30	16
10	2.42	36S	712 ± 36	0.40 ± 0.12	24	1.2	0.33	20
9	5.25	48S	814 ± 32	0.45 ± 0.09	52	1.5	0.30	35
8	49.09	66S	961 ± 38	2.42 ± 0.41	483	2.4	1.00	201
7	48.83	5,479[a]	707 ± 24	7.74 ± 1.55	457	5.0	1.55	91
6	0.99	15,800[a]	751 ± 72	0.12 ± 0.06	9	5.0	0.02	2

[a] Apparent height of pixel center above jovian limb.

TABLE IV
3 May 1993: 4.0-μm Dataset Taken at CML of 196

Row	I(3.533 μm) (10^{-13} erg cm^{-2})	Lat. (km)	T(K)	$N(H_3^+)$ (10^{12} cm^{-2})	$E(H_3^+)$ (10^{-3} erg sec^{-1} cm^{-2} sr^{-1})	L.S.	$N(H_3^+)$* (10^{12} cm^{-2})	$E(H_3^+)$* (10^{-3} erg sec^{-1} cm^{-2} sr^{-1})
21	4.60	10,484[a]	918 ± 82	0.17 ± 0.07	35	5.0	0.03	7
20	67.77	183[a]	917 ± 32	2.60 ± 0.39	530	5.0	0.52	106
19	25.07	56N	1089	0.30	125	1.2	0.17	71
7	74.27	183[a]	974 ± 48	1.49 ± 0.30	396	5.0	0.30	79

[a] Apparent height of pixel center above jovian limb.

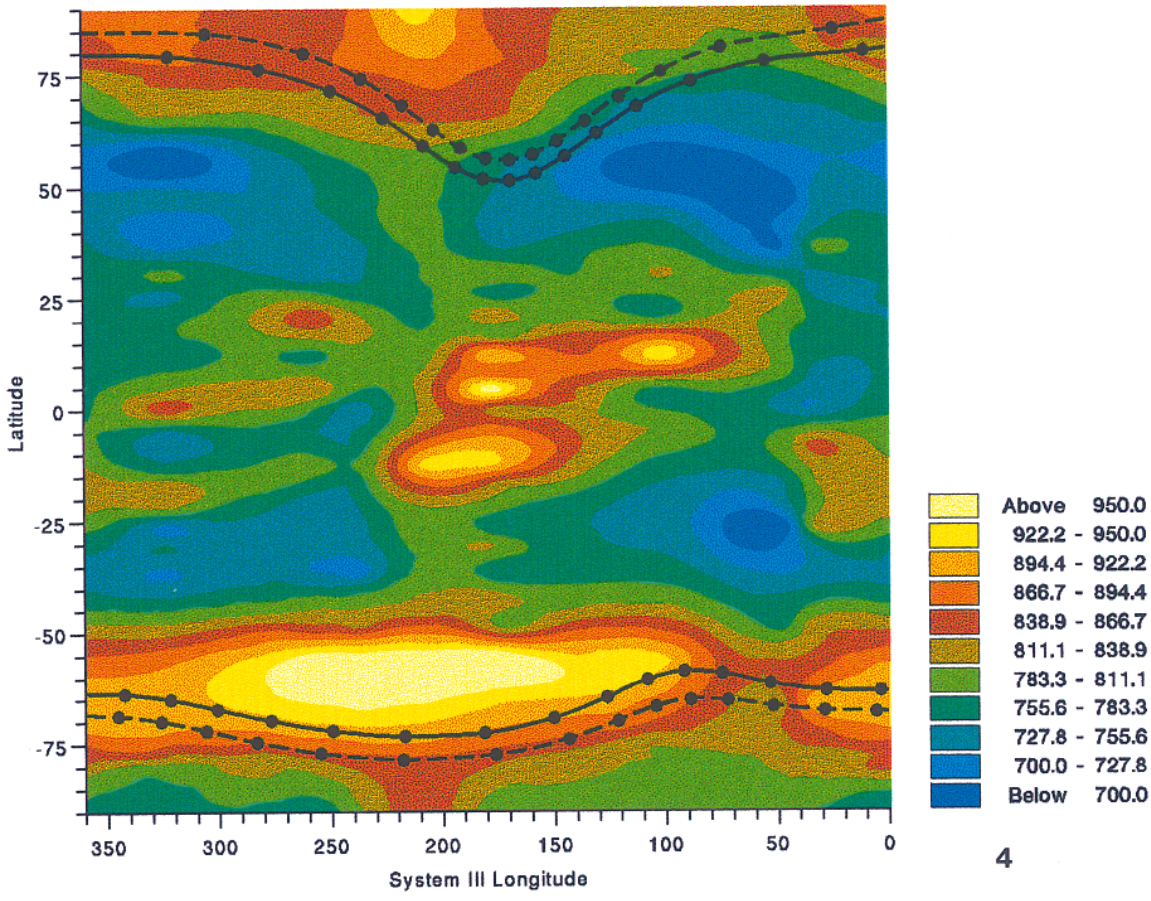

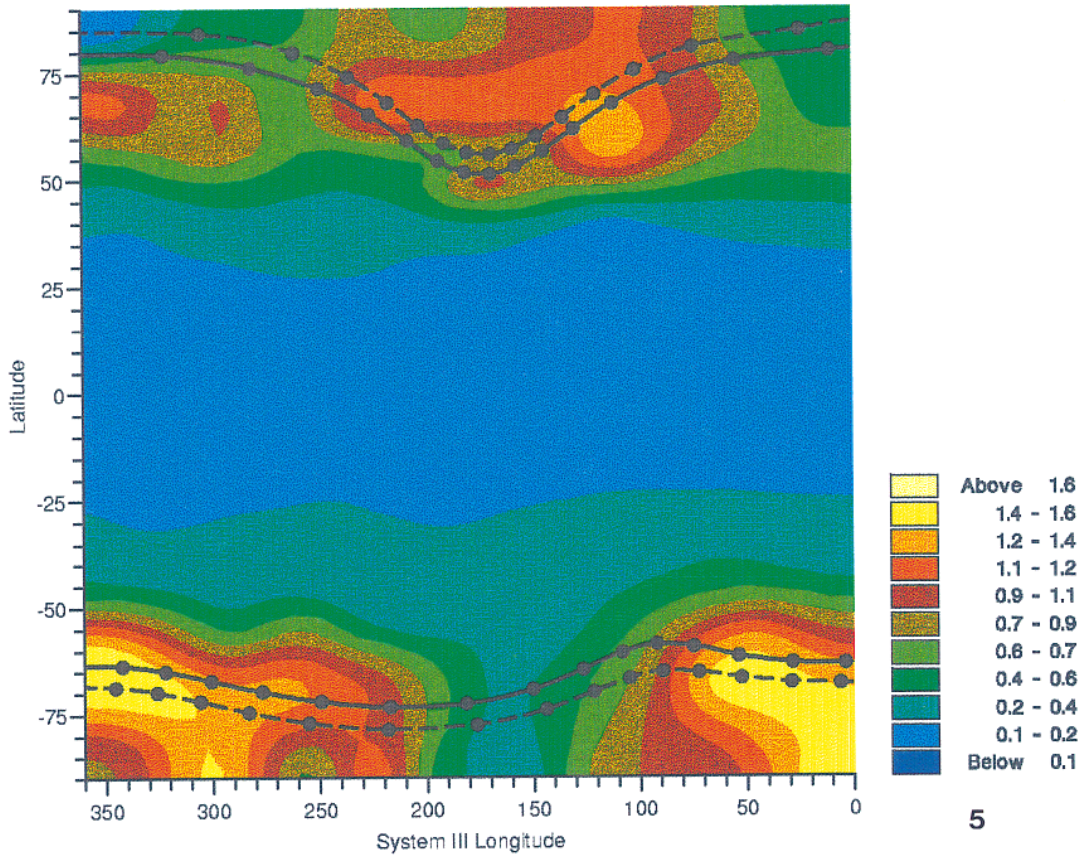

FIG. 4. Map of fitted temperatures as a function of jovian longitude and latitude. The loci of the last closed field line (broken line) and Io footprint (solid line) (as defined by Connerney 1993) are shown.

FIG. 5. As in Fig. 4 for fitted column density (corrected for line-of-sight effects). Units are 10^{12} cm^{-2}.

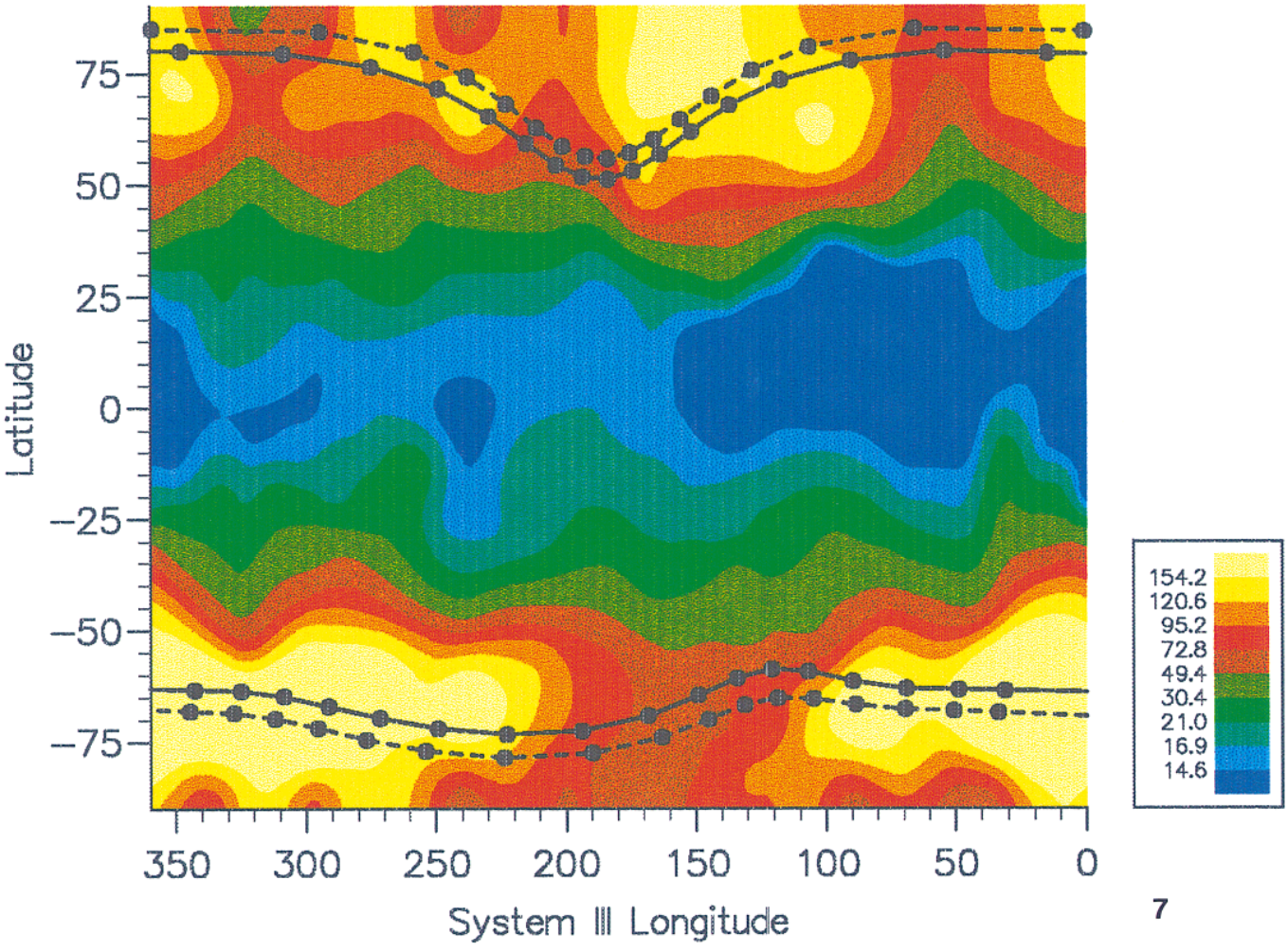

FIG. 7. Map of total emission parameter $E(H_3^+)^*$ derived from fitted temperature and column densities. Units are ergs $\times 10^{-3}$ sec^{-1} cm^{-2} sr^{-1}.

north, if we divide the auroral region roughly into 0°–180° and 180°–360°, then the first region has higher column densities but lower temperatures, and the second, higher temperatures and lower column densities. This anticorrelation between $T(H_3^+)$ and $N(H_3^+)$ is discussed in the next section.

Total H_3^+ Emission: $E(H_3^+)$

The errors in $T(H_3^+)$ and $N(H_3^+)$ reported in Tables II to V have been obtained by standard techniques, but they do not give the full extent of the potential range of the parameters that may be fitted to a single spectrum. This

TABLE V
5 May 1993: 4.0-μm Dataset Taken at CML of 202

Row	I(3.533 μm) (10^{-13} erg cm^{-2})	Lat. (km)	T(K)	$N(H_3^+)$ (10^{12} cm^{-2})	$E(H_3^+)$ (10^{-3} erg sec^{-1} cm^{-2} sr^{-1})	L.S.	$(H_3^+)^*$ (10^{12} cm^{-2})	$E(H_3^+)^*$ (10^{-3} erg sec^{-1} cm^{-2} sr^{-1})
21	4.07	10795[a]	974 ± 151	0.12 ± 0.07	32	5.0	0.02	7
20	49.37	453[a]	904 ± 45	1.87 ± 0.35	357	5.0	0.37	73
8	31.37	56S	981 ± 128	0.64 ± 0.34	175	1.8	0.36	100
7	34.57	453[a]	989 ± 54	0.98 ± 0.21	278	5.0	0.20	57

[a] Apparent height of pixel center above jovian limb.

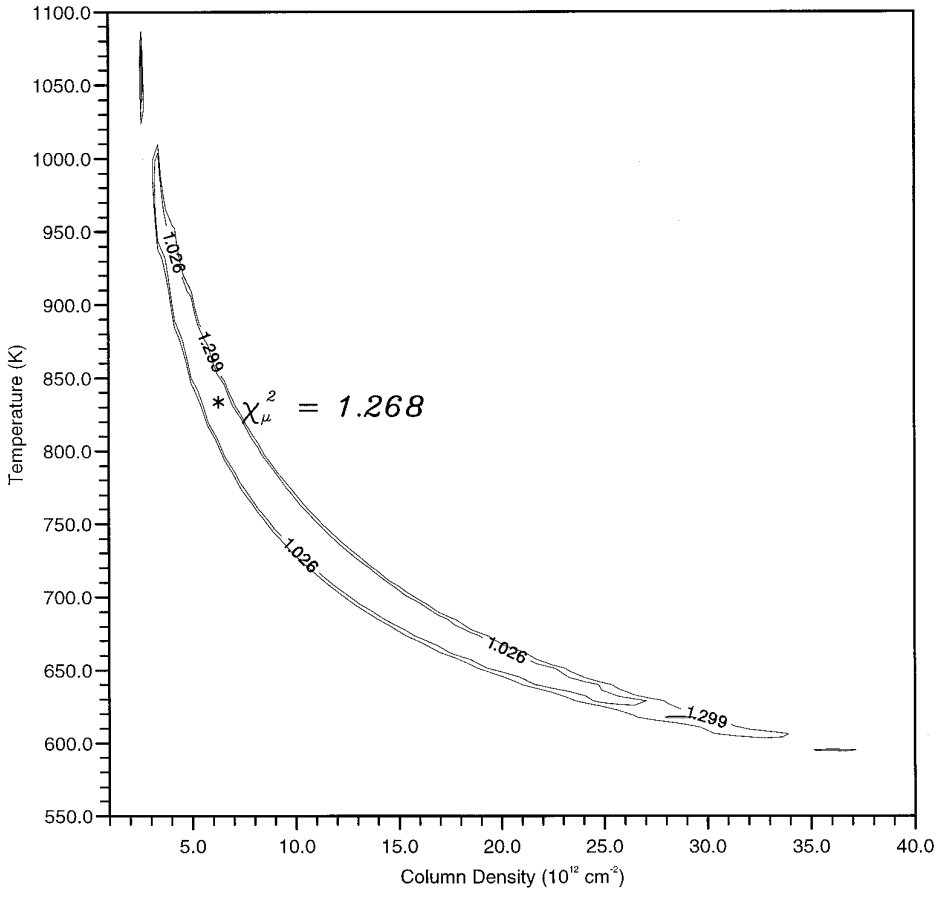

FIG. 6. χ^2–χ^2_μ contours for temperature/column density parameters derived from a typical auroral spectrum, covering the 2σ (95% confidence level) and 3σ (99% confidence level) error levels. For the given value of $\chi^2_\mu = 1.268$ obtained from the fit, $\chi^2 - \chi^2_\mu = 1.026$ corresponds to the 95% confidence level, and $\chi^2 - \chi^2_\mu = 1.299$ to the 99% level.

is because $T(H_3^+)$ and $N(H_3^+)$ are 99% anticorrelated in our fits, and the minimum reached by the least-squares process is very shallow. If instead of obtaining the error in $T(H_3^+)$ by fixing it at its fitted value and allowing $N(H_3^+)$ to vary (and vice versa), both parameters are allowed to vary within the 3σ (99%) confidence limit, a contour is produced such as that shown in Fig. 6. At its limits, the temperature ranges over ± 150 K about the fitted value of $\sim$840 K and the column density from -50 to $+150$% of the least-squares minimum at $\sim 5 \times 10^{12}$ cm^{-2}. This gives a range of uncertainty for $T(H_3^+)$ and $N(H_3^+)$, taken as a pair, somewhat greater than that attributable to the individual parameters.

We therefore define a parameter $E(H_3^+)$, which gives the total emission across all wavelengths for this ion. $E(H_3^+)$ may be obtained by combining $T(H_3^+)/N(H_3^+)$ pairs provided by the least squares fitting program, and assuming that the H_3^+ emission can be modeled by assuming LTE. This latter assumption is a very good approximation for the following reasons:

1. Although the model of Kim *et al.* (1991) predicts that there should be an overabundance of ground-state H_3^+, this level contributes almost nothing to the overall emission, since the molecule has no permanent dipole. Both perturbational (Pan and Oka 1986) and full quantum mechanical (Miller and Tennyson 1988) calculations show the rotationally induced dipoles are very small ($\sim 10^{-3}$–10^{-2} Debye).

2. Further, on account of these low dipole moments, within each vibrational level rotational thermal equilibrium should be well established even at the relatively low ($\sim 10^{13}$cm^{-3}) overall number densities that prevail where H_3^+ is the major ion.

3. Finally, at typical ionospheric temperatures between 800 and 1000 K, as detailed above, 90% of all H_3^+ emission is due to the $\nu_2 \rightarrow 0$ fundamental band, and nearly all the rest to the $2\nu_2 \rightarrow 0$ overtone. Miller *et al.* (1990b) showed these bands to emit in accordance with an essentially thermal ratio. (N.B. H_3^+ has no electronic spectrum.)

We have computed the LTE emission per H_3^+ molecule using the linelist of Kao *et al.* (1989) augmented with additional transitions (Neale *et al.* 1996). (This curve is available from the authors on request.) From this, values of $E(H_3^+)$ may be determined by reading off the emission per molecule at the relevant temperature and multiplying by $N(H_3^+)$. Taking the limits of the parameters given in Fig. 6, $T(H_3^+)$ = 990 K and $N(H_3^+)$ = 2.6 x 10^{12} cm^{-2}, and $T(H_3^+)$ = 700 K and $N(H_3^+)$ = 12.0 x 10^{12} cm^{-2}, we obtain $E(H_3^+)$ = 0.73 and 0.63 erg sec^{-1} cm^{-2} sr^{-1}, respectively. This shows that $E(H_3^+)$ for T/N pairs that fall within the 3σ domain is determined to better than $\pm 10\%$. If the error in the observed line intensity ($\pm 5\%$ for the auroral regions, $\pm 10\%$ for the rest of the planet) is added to this, $E(H_3^+)$ should be stable to within $\pm 15\%$ for this auroral study. While it may be disappointing to have to give up some of the detailed physical insight given by $T(H_3^+)$ and $N(H_3^+)$ as a function of planetary position, the positive advantage of combining these parameters to give $E(H_3^+)$ is that, using it, we can now obtain information about the total emission coming from the jovian infrared auroras.

In Fig. 7 we plot the total emission corrected for line-of-sight effects, $E(H_3^+)^*$, as a function of planetary position. In the southern auroral zone, the pixel-averaged emission peaks at ~0.26 erg sec^{-1} sr^{-1} cm^{-2} between 300° and 360°, having reached a minimum around 200° to 250°. In the north, the pixel-averaged emission reaches a maximum of ~0.16 erg sec^{-1} cm^{-2} sr^{-1} around 150° and shows a number of secondary maxima. Particularly in the northern polar region, it is very noticeable that the emission is significantly above zero at the pole for all longitudes. We discuss this later.

Optical Thickness

In the previous two subsections, we made the standard assumption that H_3^+ emission is optically thin. We may test this assumption by taking values of $T(H_3^+)$ and $N(H_3^+)$ derived from our fits and applying the standard formula for optical depth. We use

$$\begin{aligned}\tau_{\nu 2} &= \int \rho_{H3+}(z)\alpha(z)[1 - \exp(-h\nu_2/kT(z)]\, dz \\ &= N(H_3^+)\alpha[1 - \exp(-h\nu_2/kT(H_3^+)] \\ &= N(H_3^+) \times [c/\nu_2]^2 \times [g_{\nu 2}/g_0] \times A_{\nu 2 \to 0} \\ &\quad \times [1 - \exp(-h\nu_2/kT(H_3^+)] \times [c/\nu_2][m/kT(H_3^+)]^{1/2},\end{aligned} \tag{1}$$

where we have substituted for α, the column averaged opacity, in the usual way, using $A_{\nu 2 \to 0}$ is 128.8 sec^{-1} and ν_2/c is 2521.3 cm^{-1} (Dinelli *et al.* 1992). We have also assumed that thermal broadening is the main contribution to the linewidth. For the situation of relatively high column density, 7.60×10^{12} cm^{-2}, and low temperature, 766 K (row 7 of Table II), we get an optical depth of 0.240; for the situation of relatively low column density, 0.64×10^{12} cm^{-2}, and high temperature, 981 K (row 8 of Table V), we get an optical depth of 0.028. In both these cases the gas is optically thin ($\tau < 1$).

But Drossart has recently pointed out (private communication) that in the auroral regions this may be misleading, for two reasons: (1) the overabundance of ground-state H_3^+ will make the gas optically thicker than the column density derived spectroscopically would indicate; (2) column densities derived spectroscopically are averages over large pixels which mask the narrow arclike nature of the brightest emission, again leading to an underestimate of the true column density. It is therefore important to consider the column densities given above as effective densities. Detailed analysis is required to relate these to model profiles. $E(H_3^+)$, in this situation, remains a reliable indicator of the atmospheric cooling due to H_3^+.

Auroral H_3^+ Emission as a Function of Longitude: E(CML)

In the previous two sections, we presented values of $T(H_3^+)$, $N(H_3^+)$, and $E(H_3^+)$ as functions of jovian location. These show that the emission is strongly concentrated around the auroral regions, with temperatures somewhat higher than in the nonauroral ionosphere. The values reported are, however, pixel averages covering a large area of the planet and can mask small, but very bright, emissions. Recently, auroral infrared images, with typical plate scales of 0.15″, have been interpreted as being due to a relatively narrow auroral oval with other, more diffuse emissions superimposed on it (Satoh *et al.* 1996). Our spectra are much less spatially sensitive, and we are not able to distinguish such features.

An alternative approach that is applicable to these data is to account for all the H_3^+ emission that falls within the slit from the auroral oval to the limb of the planet. To do this we define a parameter $E(\mathrm{CML})$. This is defined as the integral of $E(H_3^+)^*$ (averaged over the width of one pixel) along a 1-cm-wide arc following the central longitude meridian from the lowest latitude point of the auroral oval to the limb of the emission:

$$E(\mathrm{CML}) = \int_{L\sim 6}^{\mathrm{Limb}} E(H_3^+)^*(r)\, dr, \tag{2}$$

and r is the actual arc following the central longitude meridian along the surface of the planet.

In the approximation that H_3^+ emission is optically thin, for an emission shell of uniform thickness the line-of-sight correction at any point on the planet introduces a factor that is balanced by the increasing pathlength along the central meridian which subtends 1 arcsec on the slit. Thus,

$$E(\mathrm{CML}) = \int_{L\sim 6}^{\mathrm{Limb}} E(\mathrm{H}_3^+)^*(r)/\cos\gamma\cos\gamma\, dr = \int_{L\sim 6}^{\mathrm{Limb}} E(\mathrm{H}_3^+)(l)\, dl, \quad (3)$$

where l is the distance projected onto the plane at Jupiter and γ is the latitude. In practice, therefore, the value of E(CML) is obtained, in units of erg sec^{-1} cm^{-1} sr^{-1}, adding the values of the uncorrected $E(\mathrm{H}_3^+)$ for the rows spanning the auroral to limb region and multiplying by the distance spanned by one pixel (~9800 km, for these data).

Comparison with Simple Geometric Model

In theory, it should be possible to predict values for E(CML) from a complete model of the auroral regions. As yet, however, such a model is unavailable, and one role of data such as those presented here is to provide appropriate input and constraints for attempts to develop one. The E(CML) parameter is an appropriate way of doing this with data of limited spatial resolution. As a first approximation, the variation of E(CML) with System III longitude might be modeled with the following assumptions: (1) that the auroral emission region is an annulus of uniform thickness, whose inner and outer edges follow the last closed field line and $6R_J$ magnetic footprints, respectively; (2) that the emission per unit volume of the annulus is uniform. This model showed that, dependent on the aspect of the uniform annulus presented, one either sees a thin emission area of high apparent intensity due to an elongated emission pathlength or a wider area of lower-intensity emission. Additionally, in the northern hemisphere, for some CMLs it is possible to see the entire annulus as the furthermost part rises above the limb of the planet. This is due to the asymmetry of the auroral oval with respect to the rotational pole. Predicted values of E(CML) may be obtained by summing the total visible annulus volume that is contained within the slit, in this instance 3.08″ wide, and multiplying by an intensity per unit volume.

Predicted values of E(CML) are shown (in arbitrary units) in Fig. 8 for both hemispheres, along with the values obtained from the data taken during our run, as a function of the CML at which observations were made. H_3^+ emission levels are known to be highly variable, with time scales as short as 1 hr possibly being involved (Baron *et al.* 1991). Combining 3 days' data is therefore intrinsically problematic, since overall emission levels may vary from day to day. For instance, there is evidence in our dataset that levels on May 4 were somewhat higher than on the other 2 days. Nonetheless, where we have data at similar CMLs for more than 1 day, they generally overlap within the uncertainty limits. The value derived from Ballester and colleagues' (1994) study is also in good agreement with

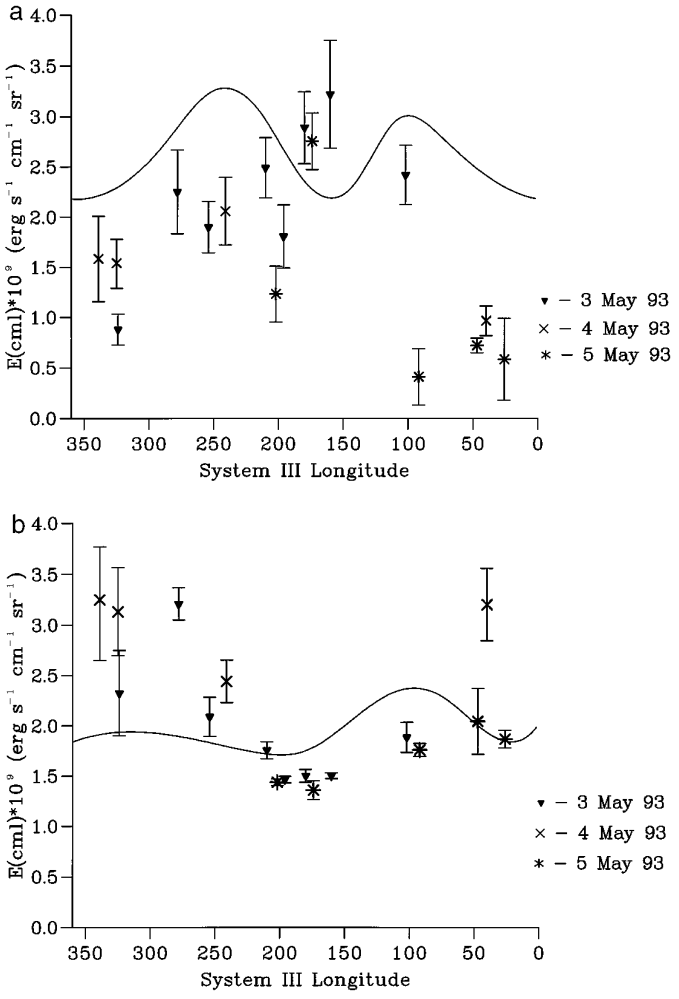

FIG. 8. Model and observed values of E(CML) as a function of CML for (a) the north and (b) the south. The units of the model values are arbitrary.

the current dataset. As with the $E(\mathrm{H}_3^+)^*$ map, the E(CML) values show considerable longitudinal variation.

For the north (Fig. 8a), the uniform annulus model predicts two relative maxima, at 100° and ~240°, where the intensity should be about 50% greater than at the minima. The actual data show two maxima, but at 150° and then a broader peak extending from ~210° to 280°. Moreover, the range of E(CML) values extends over nearly an order of magnitude, from 0.1×10^9 erg sec^{-1} cm^{-1} sr^{-1} at CML = 92° to 1.1×10^9 erg sec^{-1} cm^{-1} sr^{-1} at CML = 160°—much greater variation than predicted by the uniform annulus model. This is repeated in the south, where the uniform annulus model predicts even less relative variation. For the southern hemisphere, the data show the local maximum of E(CML) to be about 180° out of phase with the north, with values varying from 0.4×10^9 erg sec^{-1} cm^{-1} sr^{-1} at CML = 174° to ~1.1×10^9 erg sec^{-1} cm^{-1} sr^{-1}

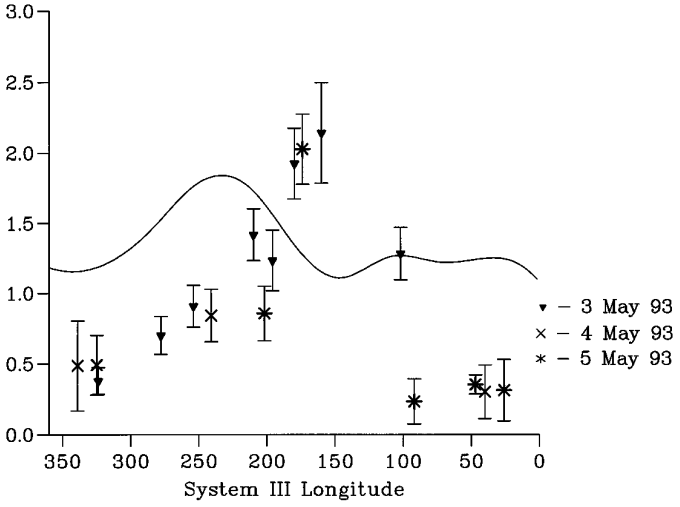

FIG. 9. Model and observed values of the north/south ratio of E(CML).

in the region of CML = 339–340°. UV data show that it may be necessary to introduce a longitude shift to get models and observations to agree (Prangé and Elkhamsi 1991). There is also some evidence for this in our data.

North/South Ratio

The longitudinal variation of the auroral emission may be investigated further by looking at the ratio between the northern and southern intensities. This has an additional advantage in that day-to-day variations can be minimized, since previous investigations have shown that overall hemispheric auroral brightness variations are positively correlated (Livengood *et al.* 1992). The north/south ratio is shown in Fig. 9, where the ratio predicted by the uniform annulus model is superimposed on the values obtained from our data.

The data do, indeed, indicate that daily variations in overall magnitude have no significant effect on N/S as a function of longitude. What is striking about the observed data is that N/S varies by nearly an order of magnitude from 0.25 at CML = 92° to 2.3 at CML = 160°. The uniform annulus model predicts a much more restricted range of values, however, from 1.1 at CML = 150° to 1.9 at CML = 240°. As expected, therefore, the first-order approximation we have made is not a good representation of the real jovian auroral behavior.

Various factors could account for this:

1. There is no a priori reason why the emission per unit volume of the annulus should be uniform.

2. There is an extended region of UV diffuse emission straddling the northern auroral arc centered on System III Longitude 150° (Clarke *et al.* 1995, Prangé *et al.* 1995). If this has an infrared counterpart, this may account both for the peak in the north at this longitude and the resulting high N/S ratio.

3. The UV images also show that lower-level emission occurs across the polar region inside of the auroral oval (Dols *et al.* 1992).

At the spatial resolution of our pixel size, however, it is not possible to separate these factors in the way that is now being attempted for IR images (Satoh *et al.* 1996). Nonetheless, information that is both useful and complementary to the imaging data can be obtained. Baron *et al.* (1996) have suggested that measuring the total flux from IR images as a function of the observing CML is a useful way of monitoring the activity of the auroras. In particular they have suggested that emission levels vary according to the ram pressure of the solar wind. Their data also show that temporal variations in northern and southern emission levels are positively correlated. Our use of E(CML) is similar in concept to their proposal, but has two advantages:

1. It is slightly more spatially discriminating in that we have a slit that cuts out emission from the points on the rising and setting limbs where the auroral ovals disappear behind the planet (although it does not cut out emission from the furthermost part of the ovals which appear over the polar limb). Emission from the rising and setting limbs can be a significant fraction of the total emission, and tends to damp out genuine longitudinal variations.

2. More importantly, our use of the $E(H_3^+)$ parameter to obtain E(CML) enables us to evaluate the total emission due to the IR auroras. This is difficult to obtain from images obtained using (typically) a spectral resolution of 1–2% of the central wavelength. In such cases, all one can state is that the intensity in such a wavelength region is varying and make the assumption that this is valid throughout the entire spectral region in which H_3^+ emits.

Total H_3^+ Auroral Emission

Since our data give good longitudinal coverage of the planet, we are in a position to compare the total auroral output due to H_3^+ emission in the infrared with other emission sources. To do this, we have calculated the total output by summing our values of E(CML) along the locus of the auroral uniform annulus. This process gives a total emission of 3.4 ($\pm$30%) $\times$ 10^{12} W in the north and 3.0 ($\pm$30%) $\times$ 10^{12} W in the south. (It should be noted that for some CMLs in the north, particularly around 180°, the viewing geometry means that E(CML) includes emission from the segment of the auroral oval that rises above the northern limb ($\lambda_{III} \sim 0°$) of the planet as well as that from the oval at $\lambda_{III} \sim 180°$. Since it is difficult to estimate this effect, it means that our calculation may slightly overesti-

mate the total H_3^+ northern auroral output. This, in turn, may account for the northern value obtained being slightly higher than that for the south. Local time effects may also influence the total output at any particular instant.) Our results show that the power output of the infrared auroras, calculated from the local noon values, is of a similar magnitude to that due to ultraviolet auroral emission (Livengood *et al.* 1992) and is about 10% of the infrared output due to hydrocarbons (Drossart *et al*. 1993).

CONCLUSIONS

The study presented here makes use of data obtained with what is, by today's standards, a rather small detector array. With new, larger, detector arrays it is possible to obtain greater spectral coverage and angular resolution. This, in turn, makes it possible to get more reliable fits to temperature and column density as individual parameters and to study spatial and temporal variations in more detail; however, it will still be useful to combine these parameters, as described in this paper, to produce values for the total emission parameters, $E(H_3^+)$ and E(CML). The spatial distribution of these emission parameters can then be used to yield information about the properties of Jupiter's ionosphere in the polar auroral regions and throughout the dayside hemisphere.

The N/S ratio obtained from E(CML) also appears to be a useful monitoring tool, since it can take account of fluctuations in overall auroral brightness, at least as they occur within the time scale of a few days, allowing for spatial and temporal variations to be studied separately. The behavior of E(CML) deduced from our data is consistent with UV studies that show that even for overall brightness variations of a factor of 2 or 3, northern and southern auroral emission is positively correlated (Livengood *et al.* 1992). It is therefore possible to use our N/S ratio as baseline for auroral activity against which significant deviations in behavior may be judged. (Over an extended period, however, it will be necessary to allow for changes in the jovian sub-Earth latitude.) This has already proved useful in our analysis of the post-SL9 auroral activity, which showed N/S ratios reaching almost an order of magnitude higher at some longitudes than is found in our 1993 dataset (Achilleos *et al.* 1995 and work in progress, Miller *et al.* 1995).

Over the past few years much has been learned about the exact nature—locus, power, and variability—of the jovian IR auroras. As a result it should now be possible to make use of baseline studies such as those reported here and by Baron *et al.* (1996) to monitor the behavior of these emissions, and correlate them to other physical parameters, such as magnetospheric plasma conditions. The best results will probably be obtained by the combination of spectroscopy and imaging. In principle, to make direct comparisons, the images could be manipulated to simulate the effect of using a slit to mask out these rising and setting limb effects, and the spectra could be convolved with profiles of the same spectral resolution as the images. That done, one may return to exploit the strengths of the individual techniques to obtain the deeper insights required to understand the auroras of Jupiter more fully.

ACKNOWLEDGMENTS

We express our thanks to the staff of the United Kingdom Infrared Telescope, Hawaii, for their hard work and assistance during the collection of these data. The telescope is operated by the Joint Astronomy Centre on behalf of the U.K. Particle Physics and Astronomy Research Council (formerly the Science and Engineering Research Council), which is also thanked for the award of a Ph.D. studentship to H.A.L. This paper has been substantially improved thanks to the helpful comments of Pierre Drossart and an anonymous referee, whose assistance is gratefully acknowledged.

REFERENCES

Achilleos, N., S. Miller, B.-M. Dinelli, H. A. Lam, J. Tennyson, M.-F. Jagod, T. R. Geballe, L. M. Trafton, R. D. Joseph, and G. E. Ballester 1995. Post-SL9 impact brightness imbalance in the jovian aurorae. In *Proceedings, European SL9/Jupiter Workshop* (R. West and H. Bohmhardt, Eds.), pp. 375–380. ESO, Garching bei Munchen.

Atreya, S.K. 1986. *Atmospheres and Ionospheres of the Outer Planets and Their Satellites.* Springer-Verlag, Heidelberg.

Atreya, S. K., and T. M. Donahue 1976. Model ionospheres of Jupiter. In *Jupiter* (T. Gehrels, Ed.), pp. 304–310. Univ. of Arizona Press, Tucson.

Ballester, G. E., S. Miller, J. Tennyson, T. R. Geballe, and L. M. Trafton 1994. Latitudinal temperature variations of jovian H_3^+. *Icarus* **107,** 189–194.

Baron, R., R. D. Joseph, T. Owen, J. Tennyson, S. Miller, and G. E. Ballester 1991. Imaging Jupiter's aurorae from H_3^+ emissions in the 3–4 micron band. *Nature* **353,** 539–542.

Baron, R., T. Owen, J. E. P. Connerney, T. Satoh, and J. Harrington 1996. Solar wind control of Jupiter's H_3^+ auroras. *Icarus* **120,** 437–442.

Clarke, J. T., and 19 co-authors 1995. HST far-ultraviolet imaging of Jupiter during the impacts of Comet Shoemaker–Levy 9. *Science* **267,** 1302–1307.

Connerney, J. E. P. 1993. Magnetic fields of the outer planets. *J. Geophys. Res.* **98,** 18659–18679.

Dinelli, B. M., S. Miller, and J. Tennyson 1992. Bands of H_3^+ up to $4\nu_2$: Rovibrational transitions from first principles calculations. *J. Mol. Spectrosc.* **153,** 718–725.

Dols, V. J.-C. Gerard, F. Paresce, R. Prangé, and A. Vidal-Madjar 1992. Ultraviolet imaging of the jovian aurorae with the Hubble Space Telescope. *Geophys. Res. Lett.* **19,** 1803–1806.

Drossart, P., B. Bezard, S. Atreya, J. Bishop, J. H. Waite, Jr., and D. Boice 1993. Thermal profiles in the auroral regions of Jupiter. *J. Geophys. Res.* **98,** 18803–18811.

Drossart, P., T. Encrenaz, R. Schultz, and J. A. Stuwe 1996. The spectrum of Jupiter at 3.5 μm. *Icarus* **121,** 199–201.

Drossart, P., J-P. Maillard, J. Caldwell, S. J. Kim, J. K. G. Wattson, W. A. Majewski, J. Tennyson, S. Miller, S. K. Atreya, J. T. Clarke, J. H. Waite, Jr., and R. Wagener 1989. Detection of H_3^+ on Jupiter. *Nature* **340,** 539–541.

Geballe, T. R., M.-F. Jagod, and T. Oka 1993. Detection of H_3^+ emission lines in Saturn. *Astrophys. J.* **408,** L109–L112.

Hamilton, D. C., G. Gloeker, S. M. Krimigis, C. O. Bostrom, T. P. Armstrong, W. I. Axford, C. Y. Fan, L. J. Lanzerotti, and D. M. Hunten 1980. Detection of energetic hydrogen molecules in Jupiter's magnetosphere by Voyager 2: Evidence for an ionic plasma source. *Geophys. Res. Lett.* **7,** 813–816.

Joseph, R. D., S. Ridgway, S. Miller, H. A. Lam, and J. Tennyson 1992. Spectroscopic mapping of jovian H_3^+. *Bull. Am. Astron. Soc.* **24,** 1034.

Kao, L., T. Oka, S. Miller, and J. Tennyson 1989. A table of astronomically important ro-vibrational transitions for the H_3^+ molecular ion. *Astrophys. J. Suppl.* **77,** 317–329.

Kim, Y. H., J. L. Fox, and H. S. Porter 1991. Densities and vibrational distribution of H_3^+ in the jovian auroral ionosphere. *J.Geophys. Res.* **97,** 6093–6101.

Lam, H. A. 1995. *Monitoring the Jovian Ionosphere Using H_3^+ Emission as a Probe.* Ph.D. thesis, University of London.

Lee, S. S., B. F. Ventrudo, D. T. Cassidy, T. Oka, S. Miller, and J. Tennyson 1991. Observation of the $3\nu_2 \leftarrow 0$ overtone band of H_3^+. *J. Mol. Spectrosc*. **145,** 222–224.

Livengood, T. A., H. W. Moos, G. E. Ballester, and R. Prangé 1992. Jovian ultraviolet auroral activity, 1981–1991. *Icarus* **97,** 26–45.

Maillard, J-P., P. Drossart, J. K. G. Wattson, S. J. Kim, and J. Caldwell 1990. H_3^+ fundamental band in Jupiter's auroral zones at high resolution from 2400 to 2900 inverse centimetres. *Astrophys. J.* **363,** L37–L41.

Majewski, W. A., J. K. G. Watson, P. A. Feldman, S. Miller, and J. Tennyson 1989. Laboratory observation of the $2\nu_2$ band of the H_3^+ molecular ion. *Astrophys. J*. **347,** L51–L54.

McConnell, J. C., and T. Majeed 1991. H_3^+ in the jovian ionosphere. *J. Geophys. Res*. **92,** 8570–8578.

Miller, S., and J. Tennyson 1988. Calculated rotational and ro-vibrational transitions in the spectrum of H_3^+. *Astrophys. J*. **335,** 486–494.

Miller, S., and J. Tennyson 1989. Hot band transitions in H_3^+: First principles calculations. *J. Mol. Spectrosc*. **136,** 223–240.

Miller, S., J. Tennyson, and B. T. Sutcliffe 1990a. ''Forbidden'' rotational and rovibrational transitions in H_3^+: First principles calculations. *J. Mol. Spectrosc*. **141,** 104–117.

Miller, S., R. D. Joseph, and J. Tennyson 1990b. Infrared emissions of H_3^+ in the atmosphere of Jupiter in the 2.1 and 4.0 micron region. *Astrophys. J*. **360,** L55–L58.

Miller, S., H.A. Lam, and J. Tennyson 1994. What astronomy has learned from H_3^+. *Can J. Phys*. **72,** 760–771.

Miller, S., N. Achilleos, B. M. Dinelli, H. A. Lam, J. Tennyson, M. F. Jagod, T. R. Geballe, L. M. Trafton, R. D. Joseph, G. E. Ballester, K. Baines, T. Y. Brooke, and G. Orton 1995. The effect of the impact of Comet Shoemaker–Levy 9 on Jupiter's aurorae. *Geophys. Res. Lett*. **12,** 1629–1632.

Neale, L., S. Miller, and J. Tennyson 1996. Spectroscopic properties of the H_3^+ molecule: A new calculated line list. *Astrophys. J*. **464,** 516–520.

Oka, T., and T. R. Geballe 1990. Observations of the 4 micron fundamental band of H_3^+ in Jupiter. *Astrophys. J*. **351,** L53–L56.

Pan, T., and T. Oka 1986. The forbidden rotational spectrum of H_3^+. *Astrophys. J.* **305,** 518–524.

Prangé, R., and M. Elkhamsi 1991. Modelling the precipitation and flux in the jovian auroral zones. *J. Geophys. Res.* **96** (A12), 21,371–21,389.

Prangé, R., I. M. Engle, J. T. Clarke, M. Dunlop, G. E. Ballester, W. H. Ip, S. Maurice, and J. Trauger 1995. Auroral signature of Comet Shoemaker–Levy 9 in the jovian magnetosphere. *Science* **267,** 1317–1320.

Satoh, T., J. E. P. Connerney, and R. Baron 1996. Emission source model of Jupiter's H_3^+ aurorae: A generalized inverse analysis of images. *Icarus* **122,** 1–23.

Sutcliffe, B. T., and J. Tennyson 1986. The infrared spectrum of H_3^+ and its isotopomers. *J. Chem. Soc. Faraday Trans. 2* **82,** 1151–1162.

Tennyson, J., S. Miller, and H. Schild 1993. First principles calculations on the astrochemistry and spectroscopy of H_3^+. *J. Chem. Soc. Faraday Trans*. **89,** 2155–2159.

Trafton, L., J. D. F. Lester, and K. L. Thompson 1989. Unidentified emission lines in Jupiter's northern and southern 2 micron aurorae. *Astrophys. J.* **343,** L73–L76.

Trafton, L. M., T. R. Geballe, S. Miller, J. Tennyson, and G. E. Ballester 1993. Detection of H_3^+ from Uranus. *Astrophys. J.* **405,** 761–766.

Trafton, L. M., J. C. Gerard, G. Munhoven, and J. H. Waite, Jr. 1994. High resolution spectra of Jupiter's northern auroral ultraviolet emission with the Hubble Space Telescope. *Astrophys. J*. **421,** 816–827.

Xu, L.-W., M. Rosslein, C. M. Gabrys, and T. Oka 1992. *J. Mol. Spectrosc.* **153,** 726–737.